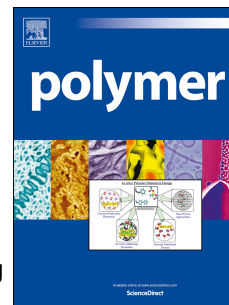


# Journal Pre-proof

The origin of memory effects in the crystallization of polyamides: Role of hydrogen bonding

Xinran Liu, Yu Wang, Zefan Wang, Dario Cavallo, Alejandro J. Müller, Ping Zhu, Ying Zhao, Xia Dong, Dujin Wang



PII: S0032-3861(19)31122-X

DOI: <https://doi.org/10.1016/j.polymer.2019.122117>

Reference: JPOL 122117

To appear in: *Polymer*

Received Date: 30 October 2019

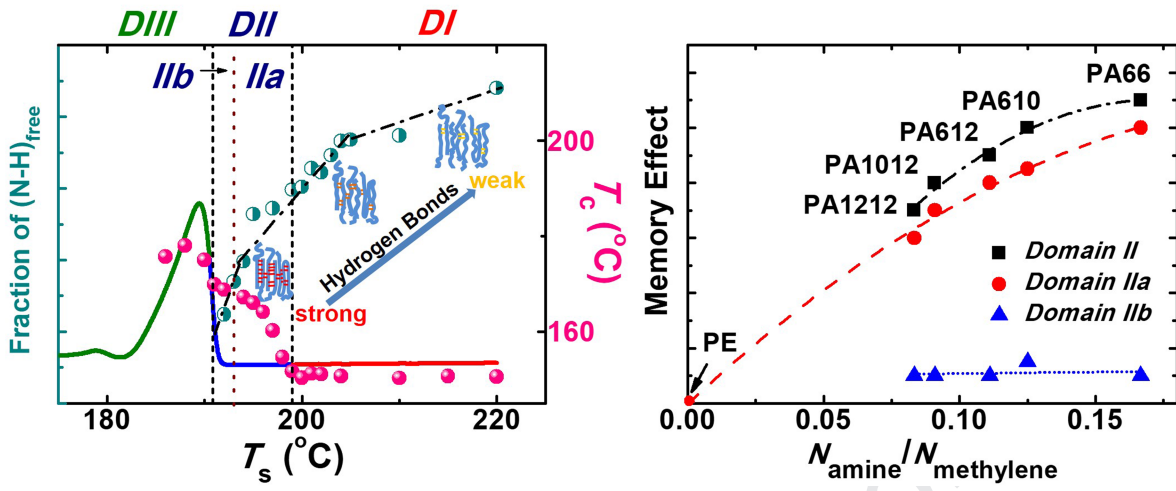
Revised Date: 13 December 2019

Accepted Date: 21 December 2019

Please cite this article as: Liu X, Wang Y, Wang Z, Cavallo D, Müller AJ, Zhu P, Zhao Y, Dong X, Wang D, The origin of memory effects in the crystallization of polyamides: Role of hydrogen bonding, *Polymer* (2020), doi: <https://doi.org/10.1016/j.polymer.2019.122117>.

This is a PDF file of an article that has undergone enhancements after acceptance, such as the addition of a cover page and metadata, and formatting for readability, but it is not yet the definitive version of record. This version will undergo additional copyediting, typesetting and review before it is published in its final form, but we are providing this version to give early visibility of the article. Please note that, during the production process, errors may be discovered which could affect the content, and all legal disclaimers that apply to the journal pertain.

© 2019 Published by Elsevier Ltd.



1 **The Origin of Memory Effects in the Crystallization of Polyamides:**  
2 **Role of Hydrogen Bonding**

3 Xinran Liu, <sup>a,b,#</sup> Yu Wang, <sup>a,c,#</sup> Zefan Wang, <sup>a,b</sup> Dario Cavallo, <sup>d</sup> Alejandro J. Müller, <sup>e,f</sup>

4 Ping Zhu, <sup>a</sup> Ying Zhao, <sup>a,b</sup> Xia Dong, <sup>a,b\*</sup> and Dujin Wang <sup>a,b</sup>

5 <sup>a</sup> CAS Key Laboratory of Engineering Plastics, CAS Research/Education Center for Excellence  
6 in Molecular Sciences, Institute of Chemistry, Chinese Academy of Sciences, Beijing 100190,  
7 China

8 <sup>b</sup> University of Chinese Academy of Sciences, Beijing 100049, China

9 <sup>c</sup> Shenzhen Key Laboratory of Polymer Science and Technology, College of Materials Science  
10 and Engineering, Shenzhen University, Shenzhen 518060, China

11 <sup>d</sup> Department of Chemistry and Industrial Chemistry, University of Genova, via Dodecaneso,  
12 31 - 16146 Genova, Italy

13 <sup>e</sup> POLYMAT and Polymer Science and Technology Department, Faculty of Chemistry,  
14 University of the Basque Country UPV/EHU, Paseo Manuel de Lardizabal 3, 20018  
15 Donostia-San Sebastián, Spain

16 <sup>f</sup> Ikerbasque, Basque Foundation for Science, Bilbao, Spain

17 <sup>#</sup> XR Liu and Y Wang contributed equally to this work.

18 \* Corresponding author: Xia Dong (xiadong@iccas.ac.cn)

19

20

## 1 ABSTRACT

2 The effect of hydrogen bonding stability on the memory effects in the  
3 crystallization of long chain polyamides have been investigated by the self-nucleation  
4 calorimetric technique. Self-nucleation is characterized by three domains in decreasing  
5 temperature order: complete melting or *Domain I*, exclusive self-nucleation or *Domain*  
6 *II* and, self-nucleation and annealing or *Domain III*. The memory effect is observed in  
7 the high temperature range of *Domain II* (when all crystals are molten, or in *Domain*  
8 *Ila*). In the low temperature range of *Domain II*, crystal remnants act as self-seeds (i.e.,  
9 *Domain I Ib*). The hydrogen bonds between amide groups were detected with FTIR, and  
10 a ratio of the content of hydrogen bonded vs. free amide groups could be calculated.  
11 The energy needed to break the hydrogen bonds decreases as the self-nucleation  
12 temperature ( $T_s$ ) increases. This means that hydrogen bonds become weaker (and their  
13 amount decrease), while the crystalline memory disappears upon crossing from  
14 *Domain I Ia* to *Domain I*. Comparing the widths of *Domain I Ia* in different polyamides,  
15 we found for the first time a clear correlation with the relative content of amide groups  
16 with respect to methylene groups in the repeat units. In conclusion, we have  
17 demonstrated that memory in polyamides is a strong function of hydrogen bonding  
18 between chain segments.

19 *Keywords:* crystalline memory, long chain polyamides, hydrogen bonding,  
20 self-nucleation

## 1 **1. Introduction**

2 The so called, “memory effect” in the crystallization of polymers has attracted great  
3 attention as a unique feature, not commonly exhibited by low molar mass crystalline  
4 substances [1-5]. The memory effect refers both to “morphological” and “kinetic”  
5 memory of a given crystalline state. In fact, on one hand after a mild melt treatment, the  
6 recrystallized superstructure bears some resemblance to the one existing before melting,  
7 in particular in relation to the location of crystalline nuclei and the relative orientation  
8 of crystallites [6]. On the other hand, the crystallization temperature upon cooling a  
9 non-isotropic melt from a relatively low temperature (i.e., when the semi-crystalline  
10 polymer is heated to a temperature just above its melting temperature for a short time)  
11 increases with respect to that of the isotropic melt (a melt state where the melting  
12 temperature is high enough, and the time remaining at that temperature long enough, to  
13 erase all memory effects and to produce a random assembly of interpenetrated random  
14 coils that are fully relaxed) [7-10].

15 The classical approach to the study of melt-memory effects in polymer  
16 crystallization is the application of the DSC “self-nucleation” protocol proposed by  
17 Fillon et. al. [2] and extensively used and reviewed by Müller and co-workers [11-13].  
18 The memory effect in crystallization has been also referred to as self-seeding or  
19 self-nucleation [5]. An increase of melting temperature or an extended duration at a  
20 specific melting temperature can reduce the re-crystallization rate [3, 12, 14]. However,

1 the above mentioned treatments do not affect the structural characteristics during  
2 recrystallization, e.g., the long period and the lamellar thickness [15-17].

3 To date, researchers have investigated the crystallization memory effect in both  
4 homopolymers and copolymers [5, 9, 14, 18-20]. The memory effects of  
5 homopolymers have been widely studied, for instance in isotactic polypropylene (iPP)  
6 [12, 14, 21], syndiotactic polypropylene (sPP) [15], polycaprolactone (PCL) [12, 22,  
7 23], and polylactic acid (PLA) [5].

8 However, the mechanism of the memory effect is still under debate. Lorenzo et al.  
9 [12], proposed that self-nuclei originated in the high temperature region within *Domain*  
10 *II* (where no trace of crystal fragments remains) are constituted by regions in the melt  
11 with the residual orientation that the chains had in the crystalline state [13]. Luo et al.  
12 [24] have postulated that memory effect comes from heterogeneities in the topological  
13 constraints and melt entanglements distribution. Muthukumar et al. [25] have  
14 established a model where all the metastable states between the isotropic melt and the  
15 final semi-crystalline state could be represented together by just one metastable state.  
16 In this state the nucleation rate is as a function of the melt temperature. Li et. al. [26]  
17 proposed that the memory effect is due to the survival of conformational order inside  
18 molten lamellae.

19 Alamo et. al. [7-9, 24, 27] performed a series of experiments on ethylene random  
20 copolymers. They found that these copolymers showed strong memory effects, even  
21 above the equilibrium melting point. This unique phenomenon may relate to the

1 partitioning of crystallizable sequences in the process of crystallization. During  
2 subsequent melting, the diffusion of these sequences will be hindered by the chain  
3 topology, therefore the transition to a randomized melt state is slowed down remarkably  
4 [8, 27]. So, in this situation the memory effect is attributed to the topological constraints  
5 in the inter-crystalline region which will affect recrystallization [28].

6 Rheological techniques have been used to detect differences between isotropic and  
7 self-nucleated melts in PP-*ran*-PE random copolymers (with compositions rich in PP)  
8 [20]. Even though, differences were not detected between isotropic and self-nucleated  
9 melts in the Newtonian viscosity or in the relaxation time, the self-nucleated melt was  
10 found to display a clear thermo-rheologically complex behaviour. Instead, the isotropic  
11 melt was thermo-rheologically simple. The authors proposed that self-nuclei in  
12 PP-*ran*-PE random copolymers were formed by clusters of chains that retained the  
13 conformations they had when they were part of the crystals.

14 Up to now, most of the studied systems are polyolefin or olefin-based copolymers  
15 [1, 3, 9, 12, 24, 29-32]. The memory effect of polyamide, polyester and other polymer  
16 systems with stronger inter-molecular interaction, such as hydrogen bonding has  
17 received less attention. In the case of poly( $\epsilon$ -caprolactone) homopolymers (PCLs),  
18 rheology has been capable of differentiating isotropic from self-nucleated melts. Both  
19 the zero-shear viscosity and entanglement modulus have significantly higher values for  
20 the self-nucleated melt in comparison to the isotropic melt, for three PCL samples with  
21 different molecular weights. The PCLs self-nucleated melts are also

1 thermo-rheologically complex in contrast to the thermo-rheologically simple behaviour  
2 of isotropic melts [22, 23].

3       Recently [23], dielectric experiments have been employed for the first time to  
4 study crystalline memory effects in PCL. A decrease of the permittivity value of the  
5 self-nucleated melt was detected in comparison with that of the isotropic melt state,  
6 hence, a small proportion of dipoles are “restricted” in the self-nucleated melt in  
7 comparison with the isotropic melt. The authors postulated that in the high temperature  
8 region of the self-nucleation domain (i.e., *Domain IIa*), when no traces of crystals can  
9 be found as they are all molten, self-nuclei are made up of regions where molten chains  
10 have residual hydrogen bonds that can survive after crystal melting, originating the  
11 memory effect detected in PCL. The correlations of the results of rheology, DSC and  
12 dielectric permittivity was remarkable [23].

13       Considering hydrogen bonds, polyamides have similarities with polyesters like  
14 PCL. According to the literature mentioned above, one would think rheology and  
15 dielectric techniques could be applied to polyamides as well. However, both  
16 polyamides and polyesters can undergo a solid state polymerization process when  
17 they are held at temperatures above  $T_g$  because of the reaction between the end groups  
18 in the amorphous regions [33]. A significant difference between polyamides and  
19 polyesters is that the equilibrium constant for polyamides is around one hundred times  
20 or more larger than that for polyesters, and thus the requirements for removal of  
21 by-products of the reaction is much less severe in the first case [34], which means that



1 the polymerization reaction occurs much easier in polyamides. Thus, the process of  
2 the polymerization combined with the possible existence of self-nuclei will give a  
3 complicated result by rheology and/or dielectric techniques in the polyamide case.  
4 Therefore, those techniques are unsuitable for investigating the memory effect in  
5 polyamides.

6 The amide groups in polyamide, with their ability to form strong hydrogen bonds,  
7 make this polymer very different with respect to the commonly investigated polyolefins.  
8 Investigation of the memory effect of polyamides should provide insights into the  
9 relationship between the polymer crystallization and the molecular structure, i.e.,  
10 chemical constitution and specific intermolecular interactions. Despite several studies  
11 on polyamides [16, 35-39], which mainly focused on the orientation induced memory  
12 effect and/or the influence on the recrystallization, the relationship between hydrogen  
13 bonding and polyamide memory effect in crystallization in the quiescent state has not  
14 been fully elucidated in the literature.

15 As an extension of our previous works on polyamides (homopolymers and  
16 copolymers) [40-46], polyamide 1012 (PA1012) is used as a model polymer in this  
17 study. It is a typical AABB-type polyamide with long methylene chain segments  
18 between two neighbor amide groups, which is polymerized by a condensation reaction  
19 between diacid and diamine. This material is an excellent engineering polyamide with  
20 superior physical properties, such as toughness, high elastic modulus, lubrication-free  
21 performance, low water absorption and adequate dimensional stability. It is extensively

1 used in industrial fields, e.g., automobile manufacturing, electronic appliances and  
2 several commodity markets [35, 47]. PA1012 is formed by a precise number of amide  
3 groups and long aliphatic segments, therefore, it can serve as a model for investigating  
4 the role of intermolecular interactions on self-nucleation. The influence of memory  
5 effects on the crystallization kinetics and on the latent structure persisting in the melt  
6 was investigated at different length scales, employing Differential Scanning  
7 Calorimetry (DSC), and Fourier Transform Infrared Spectroscopy (FTIR).

## 8 **2. Experimental section**

### 9 *2.1. Materials*

10 The Polyamide 1012 (PA1012,  $-\text{[HN(CH}_2\text{)}_{10}\text{NHCO(CH}_2\text{)}_{10}\text{CO]-}$ ) employed here is a  
11 commercial grade, supplied by Shandong Guangyin New Materials Co., Ltd. The melt  
12 flow index of this material is 16 g/10 min, determined at 235 °C according to ASTM  
13 D1238 (2.16 kg). The results of GPC in chloroform, after sample reaction with  
14 trifluoroacetic anhydride are shown in Table S1. Although the PA1012 can only  
15 dissolve in chloroform after reaction with trifluoroacetic anhydride, causing a certain  
16 difference between the true molar mass and the one measured after trifluoroacetylation,  
17 the results in Table S1 can be taken as a valid reference value. PA1012 was synthesized  
18 from decamethylene diamine and dodecanedioic acid, whose monomers are produced  
19 by a microbiological fermentation method [13, 41]. In the last part of the work, some

1 polyamide samples (PA66, PA610, PA612 and PA1212) with different amide group  
2 density, i.e., concentration of amide groups along the chain, were employed for  
3 comparison purposes. The information and thermal properties of all the samples can be  
4 found in the supporting information, Table S2. All the polyamides were dried under  
5 vacuum at temperatures between 80 and 120 °C for 12 h before the experiments. The  
6 detailed drying conditions for the different samples are in Table S3.

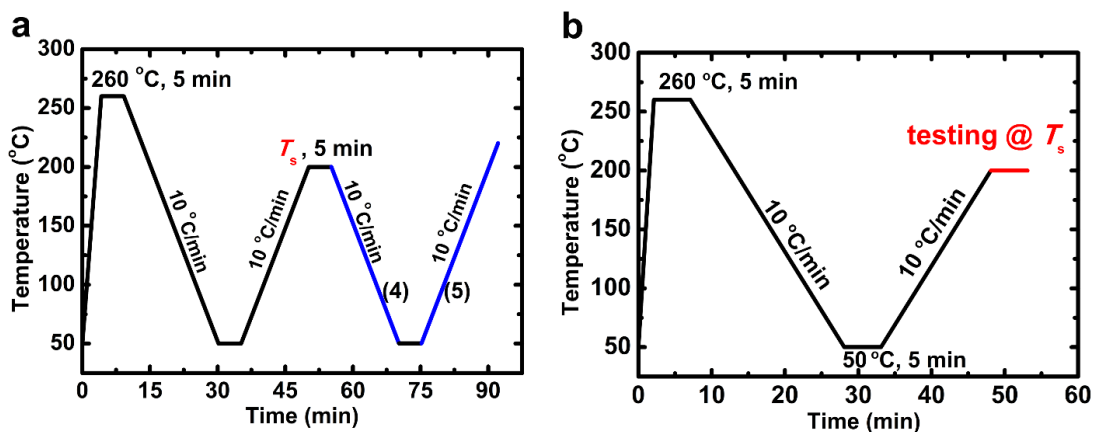
## 7 2.2. Differential Scanning Calorimetry (DSC)

8 A differential scanning calorimeter (TA Instrument, Q2000) was employed. It was  
9 calibrated with an indium standard. The sample mass employed was approximately 4  
10 mg. Samples were sealed in aluminum pans. A constant flow rate of N<sub>2</sub> was employed  
11 during the measurements.

12 (a) *Non-isothermal Crystallization*. PA1012 was characterized by a “standard”  
13 heating-cooling-heating temperature ramp. The samples were heated to 260 °C,  
14 kept in the melt for 5 min, then cooled down to 50 °C, and re-heated to 220 °C. All  
15 the heating and cooling ramps were performed at a constant rate of 10 °C /min.

16 (b) *Self-nucleation (SN) protocol*. The SN procedure was performed according to the  
17 following steps:<sup>2,12</sup> (1) Erasure of previous thermal history by holding the sample in  
18 the melt at 260 °C for 5 min. (2) Cooling from 260 to 50 °C at 10 °C/min in order to  
19 create a crystalline “standard state” in the sample. (3) Self-nucleation (SN) step,  
20 where the sample is heated to a selected temperature ( $T_s$ ) at 10 °C/min and is kept

1 for 5 min at this  $T_s$  temperature. Depending on the temperature the sample will  
 2 either completely melt (if  $T_s$  is too high, *Domain I*), it will only self-nucleate, at  
 3 intermediate  $T_s$  temperatures (in *Domain II*) or it will self-nucleate and anneal (if  
 4 the  $T_s$  temperature is too low and only causes partial melting, i.e., *Domain III*). (4)  
 5 Cooling from  $T_s$  to 50 °C at a rate of 10 °C/min. During this cooling run, the peak  
 6 crystallization temperature will be monitored to detect any changes that could  
 7 indicate an increase in its value due to self-nucleation. (5) Subsequent melting of  
 8 sample by heating from 50 to 220 °C at a rate of 10 °C/min. The SN process was  
 9 repeated at different  $T_s$  temperatures separated by 1 °C in a wide temperature range  
 10 that encompasses the entire melting range of the polymer and above (i.e., to include  
 11 all the SN domains and to determine their boundaries). In particular, the  $T_s$   
 12 temperature at which the self-nucleation is first observed (*Domain I/Domain II*  
 13 boundary) and the  $T_s$  at which the unmelted crystals undergo both annealing and  
 14 self-nucleation (*Domain II/Domain III* boundary) must be carefully detected [2, 11].  
 15 The detailed self-nucleation (SN) procedure is schematically reported in Figure 1a.  
 16



17

1 Figure 1. The thermal protocols adopted for self-nucleation experiments employing DSC (a)  
2 and *in-situ* FTIR tests (b).

### 3 2.3. Fourier Transform Infrared Spectroscopy (FTIR)

4 FTIR spectra were collected using a Nicolet 6700 Spectrometer (Thermo Fisher  
5 Scientific) in transmission mode, with an MCT detector. The spectra were measured  
6 with a resolution of  $4\text{ cm}^{-1}$  and accumulating 16 scans. The samples were films with 20  
7  $\mu\text{m}$  thickness sandwiched in between potassium bromide thin slices and mounted onto a  
8 Linkam FTIR 600 hot stage fitted in the test chamber of the FTIR to record *in-situ*  
9 spectra. Temperature calibration of the hot stage was performed with indium and tin  
10 standards. The thermal protocol was the same as that applied for the X-ray experiments  
11 (Figure 1b). In order to get the conformational information of the PA1012 film at each  
12  $T_s$ , the *in-situ* FTIR data were recorded every 30 s while holding the sample at  $T_s$ .

## 13 3. Results and discussion

### 14 3.1. Melt temperature regions at which memory effects can be observed.

15 The self-nucleation of PA1012 was studied according to the thermal protocol described  
16 in Figure 1a. Selected DSC curves recorded during cooling from the indicated  $T_s$   
17 temperatures and also during the subsequent heating scans are shown in Figure 2. From  
18 the DSC scans presented in Figure 2, the SN domains can be easily obtained [2, 11].

19

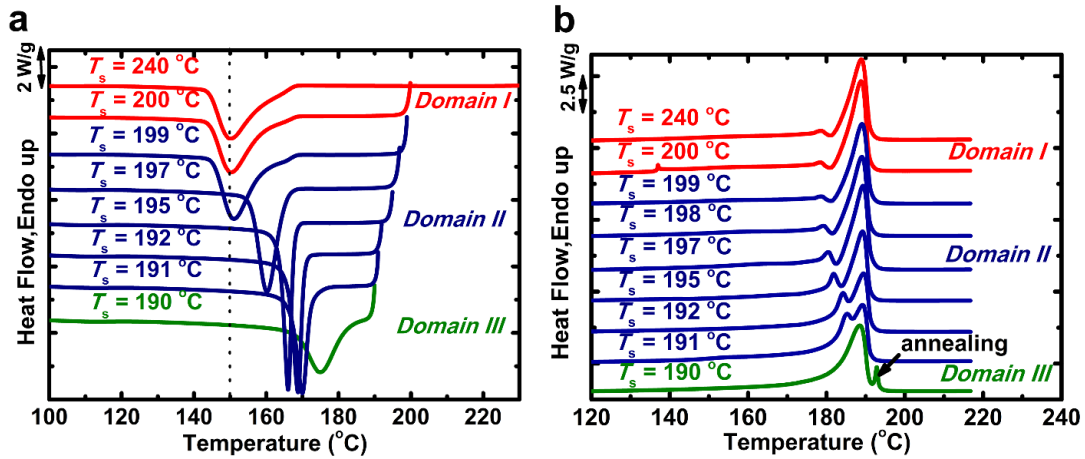


Figure 2. DSC cooling (a) and heating (b) scans of PA1012 after self-nucleation at the indicated

$T_s$ .

The memory effect of previous crystalline structure is erased when PA1012 is heated above 199 °C. For this temperature range, the melt is in *Domain I* and the peak crystallization temperature is approximately 150 °C and does not change when the  $T_s$  is further increased, as the nucleation density remains constant.

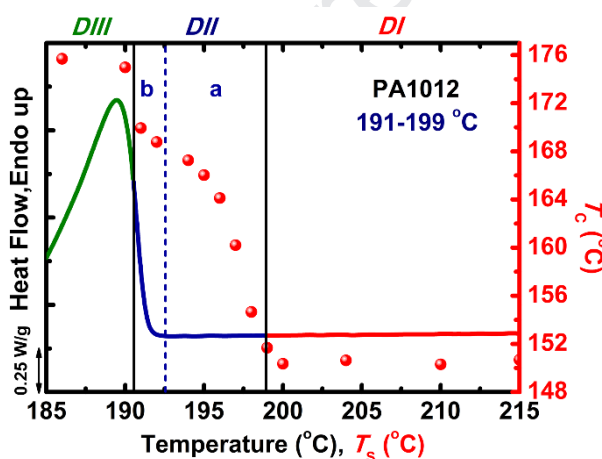
For temperatures lower than 200 °C, but higher than 190 °C, the sample is in the self-nucleation domain, or *Domain II*. The nucleation density is exponentially increased as the  $T_s$  temperature decreases, as a result of the large number of self-nuclei produced by the SN thermal protocol [2, 11]. The peak crystallization temperature increases 20 °C with respect to that in *Domain I*.

When the self-nucleation temperature ( $T_s$ ) is equal to 190 °C or lower, the sample is in the self-nucleation and annealing domain or *Domain III*. The DSC heating scan in Figure 2b for a  $T_s$  of 190 °C shows that a new melting endotherm develops: it is a sharp but small second melting peak located at higher temperatures. This corresponds to the

1 melting of a small crystal population that was not molten at 190 °C, and had time to  
 2 anneal during the 5 min waiting period at that temperature (i.e., the crystalline lamellae  
 3 thickened at 190 °C and therefore melt at temperatures higher than 190 °C). This  $T_s$  of  
 4 190 °C represents the upper temperature boundary of *Domain III*.

5 In Figure 3, the recorded peak crystallization temperatures are represented as a  
 6 function of employed self-nucleation temperatures, and compared with the “standard”  
 7 DSC melting curve of PA1012. In this way, it is possible to derive the location of the  
 8 domain boundaries with respect to the melting range of the preexisting crystals.

9



10

11 Figure 3. The self-nucleation domains (vertical lines indicate the limits between domains and a  
 12 color code in the DSC trace has also been employed to differentiate the domains: red for  
 13 *Domain I*, blue for *Domain II* and green for *Domain III*) for PA1012 represented on the standard  
 14 DSC melting trace. Data points represent the crystallization temperature peaks (plotted using  
 15 the right-hand y-axis) as a function of  $T_s$  values (on the x-axis). The dotted vertical line divides  
 16 the *Domain II* into two regions: the higher temperature region “*Domain IIa*” and the lower

1 temperature region “*Domain IIb*”.

2

3 It can be seen that the boundary between the *Domain III* and *Domain II* is located  
4 slightly within the high-temperature tail of the standard melting endotherm. The end of  
5 the melting peak is about 2 °C higher than the boundary temperature between *Domain*  
6 *III* and *Domain II*.

7 Müller et al. [11, 23] have proposed that *Domain II* should be divided into two  
8 regions. The region starting at temperatures higher than the end of the melting  
9 endotherm is “*Domain IIa*”, or memory effect domain, where all crystals have melted,  
10 but the melt still shows a crystalline memory behavior. This self-nucleated melt is not  
11 isotropic, thereby producing self-nucleation upon cooling from that  $T_s$  temperature  
12 range (i.e., upper temperature region of *Domain II*, or *Domain IIa*). The nature of the  
13 self-nuclei in *Domain IIa* is unknown for PA1012, and finding out their constitution is  
14 one of the aims in this work.

15 The lower temperature region of *Domain II* is defined as “*Domain IIb*” or  
16 “self-seeding domain” [11, 23]. In *Domain IIb*, small crystal fragments remain and they  
17 act as crystallographically ideal self-seeds (which greatly increase nucleation density  
18 upon cooling from the melt). These small crystals fragments do not anneal during the 5  
19 min spent at  $T_s$ .

20 The temperature boundary between *Domain IIa* and *Domain IIb* is about 193 °C.  
21 The width of the self-nucleation *Domain II* in PA1012 is 9 °C, indicating a moderate



1 temperature window for the existence of self-seeding (*Domain IIb*) plus memory  
2 effects (*Domain IIa*), as commonly observed for several homopolymers. For example,  
3 the width of *Domain II* in iPP is about 4 °C [2], while that of PCL is nearly 10 °C,  
4 although it can vary depending on the molecular weight and chain topology (linear  
5 versus cyclic) [11, 23]. Polymers with an intrinsically high number density of active  
6 heterogeneities (such as high density polyethylene) have a very small width of *Domain*  
7 *II* or in some cases *Domain II* is completely absent [11].

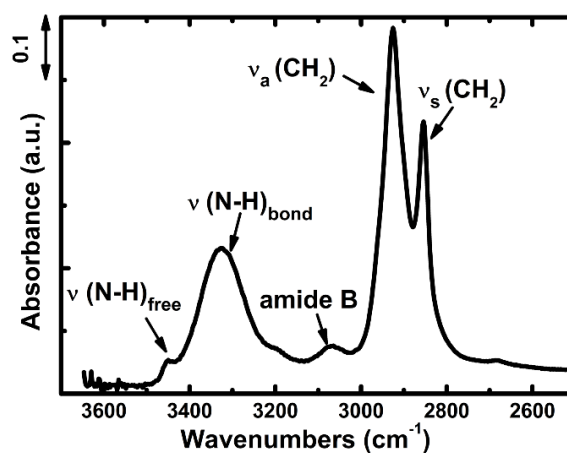
8 *Domain IIa* or the “memory effect” domain, is the most interesting to study, as this  
9 is the temperature region where memory effects cannot be simply explained by  
10 remaining crystal fragments. *Domain IIa* in homopolymers such as iPP [12] is nearly  
11 nonexistent, while in PA1012 (6.5 °C) and PCL (9.5 °C) [12], it gets much wider and is  
12 even wider in PBS (15 °C) [11]. In order to understand the origin of the memory effect  
13 in *Domain IIa*, which persists at temperatures higher than the crystals melting point,  
14 several techniques were employed to investigate the existence of order in the  
15 self-nucleated melt at different length scales.

### 16 3.2. Origin of memory effects of crystallization in PA1012

17 According to the DSC results shown in Figure 2 and Figure 3, a distinct memory  
18 effect on crystallization can be observed in the upper temperature range of *Domain II*  
19 (*Domain IIa* region) where no crystalline self-seeds remain. Further FTIR experiments  
20 were performed to determine the role of intermolecular interaction on the PA1012

1 memory effects. It is reasonable to speculate that the ordered structure causing memory  
2 effects in polyamide may be due to hydrogen bonds [16, 48], although this link is still  
3 controversial in the literature [16, 36, 48]. In the following, the vibration of the N-H  
4 group is particularly considered. Although some researchers state that the N-H  
5 stretching is not a conformational sensitive mode, since its peak position remains  
6 invariant to the change of the crystalline phase [49, 50], and the vibration band of the  
7 carbonyl group should be preferred, the latter is not chosen in this research because of  
8 its overlap with other vibration modes [50].

9 The PA1012 FTIR spectrum of the N-H stretching vibration region is shown in  
10 Figure 4, and it can be roughly resolved into three components. Two of the absorption  
11 bands can be assigned to the hydrogen bonded and free N-H stretching modes, which  
12 are marked as  $\nu(\text{N-H})_{\text{bond}}$  and  $\nu(\text{N-H})_{\text{free}}$ , respectively [50, 51]. While the one at about  
13  $3060\text{ cm}^{-1}$  corresponds to the amide B mode. The amide B is the first overtone of the  
14 amide II mode, although there is still some controversy on the origin of this band [52].  
15



16

1           Figure 4. The PA1012 FTIR spectrum of the N-H stretching vibration band.

2

3           Curve deconvolution is an accessible way to get more information from the FT-IR

4 spectra, although some inherent problems exist. Coleman et.al. [53] established criteria

5 for curve fitting of FT-IR spectrum in 1981, and afterwards many other researchers

6 referred to these rules in order to perform curve fitting on FTIR absorption bands. The

7 main issue is to establish band shape, position, width, and the number of curves

8 components comprised in a complex band, as well as the baseline, prior to the fitting

9 process [50]. In this research, the spectra base lines of the N-H stretching region (i.e.,

10 from 3120 to 3500  $\text{cm}^{-1}$ ) have been adjusted separately to obtain a more reliable result.

11 In order to know the number and positions of the curve components in this region,

12 derivative spectroscopy, which has been recognized for many years as a method to

13 enhance the resolution of small shoulders in spectra [53, 54], is applied to the N-H

14 stretching region (Figure S1). As previous researchers report that the frequency

15 difference between the “free” and hydrogen bonded N-H stretching modes is a

16 reflection of the average strength of the hydrogen bonded N-H groups [55], the width of

17 the hydrogen bonded N-H stretching band mainly reflects the distribution of hydrogen

18 bonded groups at different distances and geometries [51, 55]. For the convenience of

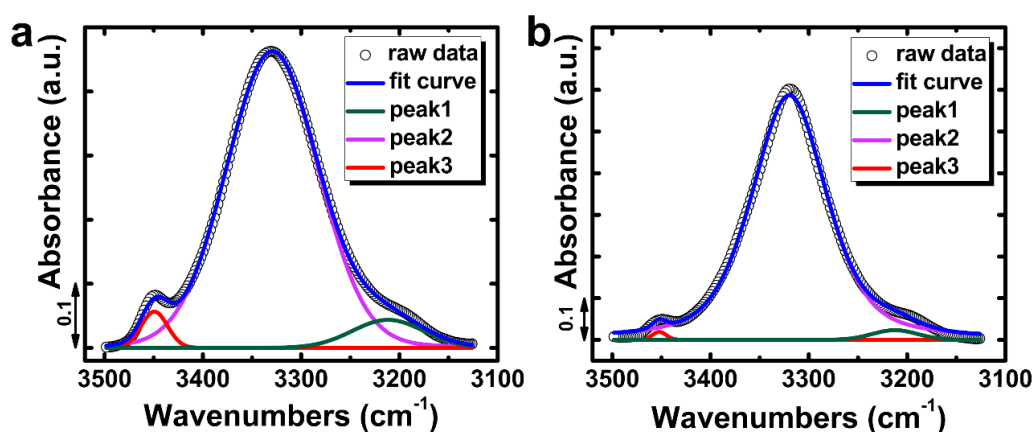
19 latter comparisons, and on the basis of the derivative spectra shown in Figure S1, three

20 different peaks have been applied for fitting this wavenumber region. Regarding the

21 employed function for curves fitting, although Gaussian function is very commonly

1 used, the results obtained with this specific peak function are not very satisfactory,  
2 especially for sample temperatures of 193 °C and below (see Figure S2). On the other  
3 hand, the Pearson VII function can yield an excellent fit (Figure S3), but the results lack  
4 an exact physical meaning. Therefore, a Gaussian/Lorentz function has been selected as  
5 more suitable for approaching the problem of curve fitting, and the results show a very  
6 small error. Obeying the above mentioned FTIR fitting rules [53] and using a set of  
7 reasonable assumptions, the N-H stretching spectrum, from 3120 to 3500  $\text{cm}^{-1}$  after  
8 normalization, has been resolved into three bands with the software PeakFit, the  
9 outcome for the peak deconvolution is shown in Figure 5 for two representative  
10 temperatures.

11



12

13 Figure 5. The N-H stretching vibration band peak fitting results at isothermal temperature of

14

220 °C (a) and 193 °C (b) with Gaussian/Lorentz function.

15

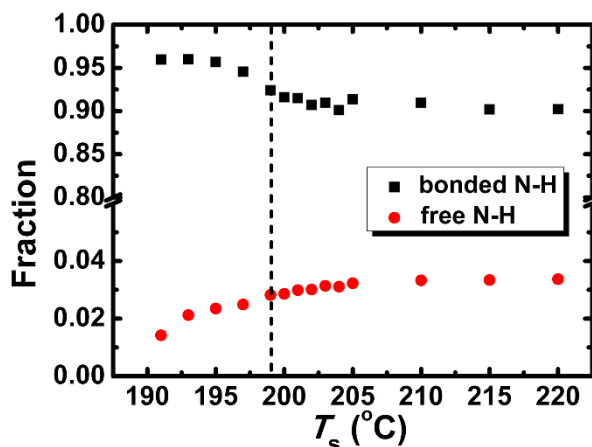
16

The data in *Domain I* is fitted with three Gaussian/Lorentz peaks and a good final

1 correlation coefficient is typically obtained. In the lower temperature range of *Domain*  
2 *II*, i.e., 193 °C and below (*Domain IIb*), the fitting results are not perfect, but still  
3 acceptable. Considering the second derivative spectra (Figure S1), two small peaks  
4 indicated with round blue circles exist at lower temperature especially in *Domain IIb*  
5 and below. The two extra-peaks at 193 °C and below may be originated by the clusters  
6 that cause the memory effect, and their presence will have an effect on the fitting  
7 quality, if only three fitting peaks are adopted. Nevertheless, despite the lower  
8 precision of the fitted curves in that temperature range, we think that the conclusion  
9 which are outlined below will not be affected. We must deduce that the state of  
10 hydrogen bonded groups in this temperature range is more complicated than that in  
11 *Domain I*, as the N-H group in the self-nucleated melt of *Domain II* is possibly  
12 experiencing a different vibrational state, or a different degree of bonding dictated by  
13 distance and geometry [50]. At a first approximation, the position of the peak is related  
14 to the strength of the interaction [50], while the peak height or peak area represents the  
15 concentration of the corresponding state. The fraction of each peak obtained by  
16 Gaussian/Lorentz fitting after holding at different  $T_s$  for 60 min are shown in Figure 6.  
17 With the addition of an antioxidant, no detectable degradation has been found during  
18 this isothermal process. According to most literature reports [40, 50, 51], we can  
19 attribute Peak 2 to the vibration of the hydrogen-bonded N-H groups, while Peak 3, at a  
20 higher wavenumber, to that of free N-Hs. Peak 1 is presumably a contribution from a  
21 two-phonon band and can be removed by the previously described curve fitting method

1 [51, 55-57].

2



3

4 Figure 6. Fraction of the fitted peaks areas as a function of  $T_s$ . The boundary temperature

5 between the *Domain I* and *Domain IIa* is indicated by the dashed vertical line.

6

7 As shown in Figure 6, the two bands only show significant changes below a  $T_s$

8 values of 200 °C, after which the fractions practically reach a plateau value. Although

9 some researchers [50] claimed that the N-H molar absorption coefficient may vary

10 with the peak position (i.e., wavenumbers), the wavenumber change with temperature

11 of each peak itself was very small compared with the difference in wavenumber

12 between the three peaks. Therefore, we can consider a constant average wavenumber

13 value during the experiment. Besides, a further approximation is to consider the band

14 area proportional to the concentration of the given NH functional group. This choice

15 seems reasonable, given that the relative variation of the absorption band is used in

16 the following calculation.

17 Under the assumption that all N-H groups in the polymer melt exist in either

1 hydrogen bonded or free state, thus a bonded-free concentration equilibrium for the  
2 N-H groups in the system can be established (Equation 1). We highlight that the word  
3 equilibrium is used to indicate an equivalence between the rates of hydrogen bond  
4 formation and dissolution, i.e., a kinetically stationary state, rather than a  
5 thermodynamic equilibrium. In fact, a continuous conversion between free and bonded  
6 N-H groups exists, as it is a dynamic process. On the other hand, the intensity and peak  
7 position of the N-H absorption band will not change when the sample is held at  $T_s$  for 60  
8 min, so it is deduced that the conversion has reasonably reached a pseudo-equilibrium  
9 concentration., and this holding time is employed for FT-IR measurements (Figure S4).  
10 Besides, the DSC cooling curves of PA1012, with a standard state, after holding at  
11 certain  $T_s$  temperature for 5 and 60 min are shown in Figure S5. The crystallization  
12 temperature  $T_c$  does not change in this time interval. Therefore, the time difference  
13 between the DSC and FTIR experiments has no influence on the obtained results.  
14 Accordingly, a dynamic equilibrium constant,  $K_g$  can be expressed by Equation 2. The  
15 equilibrium fraction of bonded N-H, which would possibly be reached after a  
16 sufficiently long holding time at  $T_s$ , depends on temperature according to Equation 3,  
17 where  $\Delta H$  represents the enthalpy difference between the free and bonded N-H states.  
18 As such, taking the area of  $\nu$  (N-H)<sub>free</sub> as the content of (N-H)<sub>free</sub>, and the areas of the  
19 other band as that of the total concentration of (N-H)<sub>bond</sub>, the equilibrium constant is  
20 shown as a function of the inverse of the absolute temperature in Figure 7.

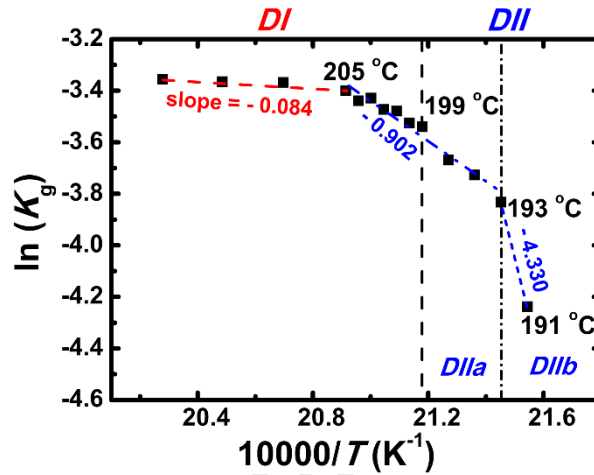
21

$$(N - H)_{bond} \rightleftharpoons (N - H)_{free} \quad (\text{Eq.1})$$

$$K_g = \frac{(N-H)_{free}}{(N-H)_{bond}} \quad (\text{Eq.2})$$

$$\ln K_g = \frac{-\Delta H}{RT} + \frac{\Delta S}{R} \quad (\text{Eq.3})$$

4



5

6 Figure 7. Natural logarithm of the equilibrium constant between hydrogen bonded and free N-H  
7 groups as a function of the reciprocal absolute temperature. The dashed vertical lines separate

8 *Domain I* from *Domain IIa* and *Domain IIb*.

9

10 Based on the different temperature dependences of  $K_g$  in Figure 7, the plot can be  
11 clearly divided into three parts. In the higher temperature range of *Domain I* (205 °C  
12 and above), the equilibrium ratio of bonded and free N-H is almost constant with the  
13 increase of  $T_s$  temperature. The temperature dependence of the equilibrium constant  $K_g$   
14 becomes stronger when lowering the temperature and it is the strongest for  
15 self-nucleation temperatures within *Domain IIb*. From the slope of the plots in the  
16 different regions, the corresponding  $\Delta H$  values are calculated (Table 1). The obtained  
17  $\Delta H$  represents the average amount of energy that the hydrogen bonded N-H groups, in



1 each identified temperature region, needs to absorb to transform into a free N-H. In  
2 other words, it shows that the stabilization of N-H groups by hydrogen bonding is  
3 strongest in *Domain IIIb* (about 360 kJ/mol) and is minimal in the high temperature  
4 range of *Domain I*, although the presence of weak hydrogen bonds was still detected (7  
5 kJ/mol). The  $\Delta H$  value in *Domain I* is perfectly in line with those obtained by other  
6 researches focusing on hydrogen bonding dynamic equilibrium in high-temperature  
7 polyamide melt [50,58], proving that our fitting procedure and the obtained results are  
8 reliable. The larger  $\Delta H$  value in *Domain II* indicates the existence of clusters  
9 maintained by the hydrogen bonds, which possess larger dissociation energy. In the  
10 low temperature region of *Domain I*, the strength of the hydrogen bond is still  
11 substantial, i.e., (75 kJ/mol), a value equal to that in *Domain IIa*, but apparently this  
12 does not affect the subsequent recrystallization of the polymer. In fact, although the  
13 strength of the hydrogen bonds is still high, the absolute content of the ordered chain  
14 aggregates is probably too low, hence no meaningful self-nucleation effect is observed.  
15 The hypothesis is confirmed in Figure S4, where the absorbance ratio between  
16  $\nu(\text{N-H})_{\text{bond}}$  and  $\nu(\text{CH}_2)$  as a function of temperature is shown. Besides, the calculation  
17 of equilibrium constant has also been done according to Gaussian and Pearson VII  
18 function, and the results are included in the Figure S7, which shows that similar trends.

19

20 Table 1. Slope of the logarithm of equilibrium constant versus reciprocal temperature and

21

calculated  $\Delta H$  for each region.

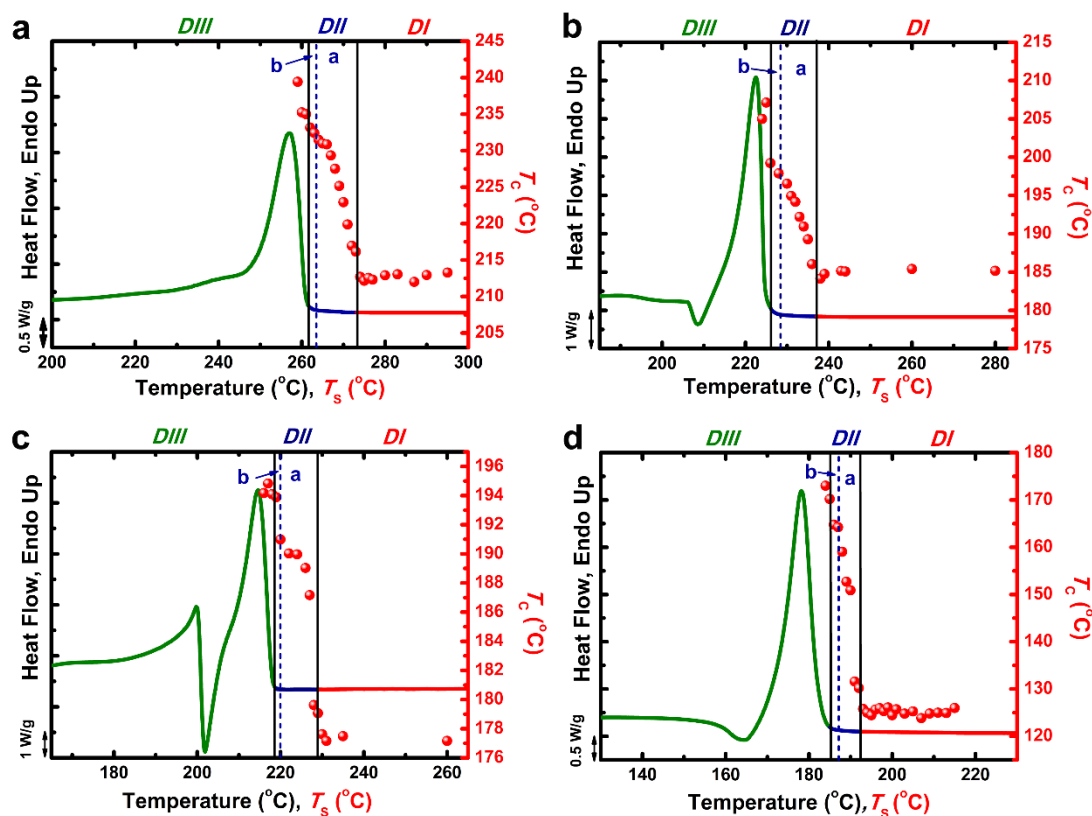
Domains Items	high temperature	low temperature	<i>DIIa</i>	<i>DIIb</i>
	range of <i>DI</i>	range of <i>DI</i>		
Slope $\times 10^4$ (K)	-0.084	-0.902	-0.902	-4.330
$\Delta H$ (kJ/mol)	7	75	75	360

1

2 Since the data collected on PA1012 indicates that hydrogen bonding plays an  
3 important role in its crystallization memory behavior, the influence of the amide group  
4 density in the repeating units of different polyamides is also investigated. Similar SN  
5 experiments were performed on PA66, PA610, PA612, and PA1212, and the different  
6 self-nucleation temperature domains are compared to the respective DSC melting  
7 endotherms in Figure 8. As expected, with the increase of average methylene sequence  
8 length in the repeating unit, the melting temperature of the polyamide drops  
9 substantially [59, 60], going from more than 250 °C for PA66 to less than 180 °C for  
10 PA1212. In parallel, the temperature range of observed memory effect also noticeably  
11 decreases, i.e., the width of *Domain IIa* (and *Domain II*) is the largest for PA66 and it  
12 gets narrower with the increase of methylene sequence lengths in the polymer repeating  
13 unit.

14

15



1

2 Figure 8. Plots of the self-nucleation domains for PA66 (a), PA610 (b), PA612 (c), and PA1212

3 (d) homopolymers, overlapped on top of the standard DSC melting traces. Data points

4 represent crystallization temperature peaks (plotted using the right-hand y-axis) as a function of

5  $T_s$  values (on the x-axis).

6

7 The widths of *Domain II*, *Domain IIa* and *Domain IIb* temperature ranges are

8 plotted against the ratio of amide groups to methylene groups of each polyamide

9 repeating unit in Figure 9. As deduced from Figure 8, the higher the concentration of

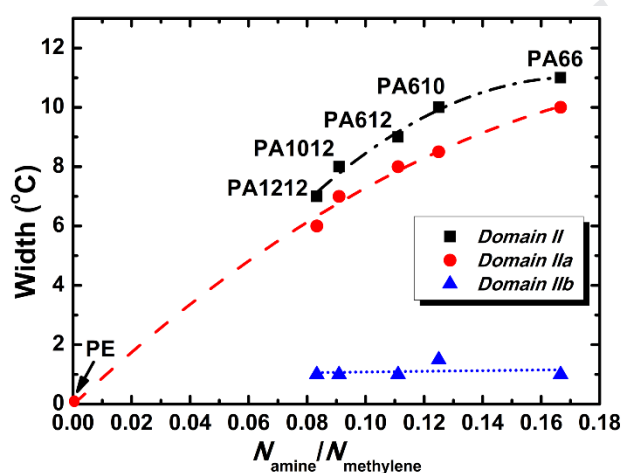
10 hydrogen bonding N-H groups, the higher the stability of the self-nuclei. A very good

11 correlation is found: the width of *Domain II* (and in particular of *Domain IIa*, where no

12 crystalline seeds are present) increases with the increase of the relative contribution of

1 amide group with respect to methylene groups within the chain. On the other hand, the  
 2 width of *Domain IIb* is unchanged by the relative content of amide groups. This  
 3 invariance indicates the predominance of crystalline self-seeds (present as unmelted  
 4 crystal fragments in *Domain IIb*) as the controlling factor of the memory effect in  
 5 recrystallization for this temperature region.

6



7

8 Figure 9. Width of *Domain II*, *Domain IIa* and *Domain IIb* as a function of the ratio of the  
 9 amide to methylene groups in the repeating units ( $N_{\text{amine}}/N_{\text{methylene}}$ ) in the different indicated  
 10 polyamides.

11

12 It is remarkable to note that, if the width of *Domain II* (or *Domain IIa*) measured  
 13 for the different polyamides is extrapolated to a zero amide groups content, a value  
 14 close to zero is obtained, consistently with the typically negligible width of *Domain II*  
 15 reported in the literature for linear polyethylene [1, 61, 62]. Therefore, while for  
 16 polyolefins the origin of intermolecular interactions existing in the self-nuclei [20]  
 17 needs further investigation, our results demonstrate that in polyamides, when the

1 density of the amide group is high, hydrogen bonding plays a dominating role in the  
2 memory effect.

3 It is conceivable that the strong chain segments interaction through hydrogen  
4 bonding slows down the achievement of an isotropic melt after the crystals have  
5 disappeared, leading to a persistent memory effect. The higher the relative content of  
6 hydrogen bonding groups in the chain repeating units, the higher the thermal energy  
7 that should be provided to break these interactions, resulting in a wider *Domain IIa*.  
8 This effect might be analogous to the known increase in viscosity and flow activation  
9 energy with concentration of hydrogen bonded groups in associative polymers [22].

10 Despite the limited amount of data for short-chain polyamides in Figure 9, it  
11 seems that the width of *Domain IIa* would reach a saturation value at high amide group  
12 contents. It can be speculated, that since the hydrogen bonds will make chain segments  
13 more rigid, if the length of the methylene chain between the amide groups is very short,  
14 the formation of chain aggregates constituting the self-nuclei after the melting of the  
15 crystalline structure (see Figure 6) might become more difficult, due to limited chain  
16 flexibility.

#### 17 **4. Conclusions**

18 In this work, the crystalline memory of a long chain polyamide, and its  
19 relationship with hydrogen bonding, was investigated. FTIR measurements performed  
20 during thermal conditioning at different self-nucleation temperatures can successfully

1 detect the presence and stability of hydrogen bonds in the studied polyamide. The  
2 variation of the ratio between free N-H and bonded N-H groups can be correlated with  
3 the dependence of the memory effect as a function of  $T_s$  values. The results show that  
4 the stabilization of N-H groups by hydrogen bonding is strongest in *Domain II* and  
5 decreases upon increasing  $T_s$  until it becomes significantly smaller in *Domain I*.  
6 Employing a series of polyamides, we were able to demonstrate that the width of the  
7 memory effect domain (*Domain IIIa*) directly correlates with the relative content of  
8 amide groups with respect to methylene groups in the repeating units. As such, it was  
9 clearly demonstrated that hydrogen bonding plays a fundamental role in the memory  
10 effects (observed in *Domain II*) of PA1012, and of long chain polyamides in general. As  
11 far as we aware, this is the first time that the key role of hydrogen bonding stability has  
12 been unequivocally linked with crystalline memory.

### 13 **Acknowledgements**

14 This work was financially supported by the National Natural Science Foundation  
15 of China (No. 21574140) and the National Key R&D Program of China (No.  
16 2017YFB0307600). The SSRF beamlines BL16B1 are acknowledged for kindly  
17 providing the beam time and assistance. We thank Dr. François Boué from CEA  
18 UMR12 Lab Léon Brillouin-Orphée Neutron Reactor for the good discussion and help  
19 on this work. We also acknowledge funding from the European Union's Horizon 2020  
20 research and innovation programme under the Marie Skłodowska-Curie grant  
21 agreement No. 778092.

## 1 Appendix A. Supplementary data

2 Figure S1-S7, Table S1-S3.

## 3 References

- 4 [1] W. Banks, M. Gordon, A. Sharples, The Crystallization of Polyethylene after  
5 Partial Melting, *Polymer* 4 (1963) 289-302.
- 6 [2] B. Fillon, J.C. Wittmann, B. Lotz, A. Thierry, Self-Nucleation and  
7 Recrystallization of Isotactic Polypropylene ( $\alpha$  Phase) Investigated by Differential  
8 Scanning Calorimetry, *J. Polym. Sci., Part B: Polym. Phys.* 31 (1993) 1383-1393.
- 9 [3] G.C. Alfonso, A. Ziabicki, Memory Effects in Isothermal Crystallization II.  
10 Isotactic Polypropylene, *Colloid. Polym. Sci.* 273 (1995) 317-323.
- 11 [4] Y.S. Zhang, L.W. Zhong, S. Yang, D.H. Liang, E.Q. Chen, Memory Effect on  
12 Solution Crystallization of High Molecular Weight Poly(ethylene oxide), *Polymer* 53  
13 (2012) 3621-3628.
- 14 [5] H. Zhang, C. Shao, W. Kong, Y. Wang, W. Cao, C. Liu, C. Shen, Memory Effect  
15 on the Crystallization Behavior of Poly(lactic acid) Probed by Infrared Spectroscopy,  
16 *Eur. Polym. J.* 91 (2017) 376-385.
- 17 [6] J. Xu, Y. Ma, W. Hu, M. Rehahn, G. Reiter, Cloning Polymer Single Crystals  
18 through Self-Seeding, *Nature Mater.* 8 (2009) 348-353.
- 19 [7] A. Mamun, X. Chen, R.G. Alamo, Interplay between a Strong Memory Effect of  
20 Crystallization and Liquid-Liquid Phase Separation in Melts of Broadly Distributed  
21 Ethylene-1-Alkene Copolymers, *Macromolecules* 47 (2014) 7958-7970.
- 22 [8] B.O. Reid, M. Vadlamudi, A. Mamun, H. Janani, H. Gao, W. Hu, R.G. Alamo,  
23 Strong Memory Effect of Crystallization above the Equilibrium Melting Point of  
24 Random Copolymers, *Macromolecules* 46 (2013) 6485-6497.
- 25 [9] X. Chen, A. Mamun, R.G. Alamo, Effect of Level of Crystallinity on Melt  
26 Memory Above the Equilibrium Melting Temperature in a Random Ethylene 1  
27 Butene Copolymer, *Mater. Chem. Phys.* 216 (2015) 1220-1226.
- 28 [10] A. Ziabicki, G.C. Alfonso, Memory Effects in Isothermal Crystallization. I.  
29 Theory, *Colloid. Polym. Sci.* 272 (1994) 1027-1042.
- 30 [11] R.M. Michell, A. Mugica, M. Zubitur, A.J. Müller, Self-Nucleation of Crystalline  
31 Phases Within Homopolymers, Polymer Blends, Copolymers, and Nanocomposites,  
32 *Adv. Polym. Sci.* 276 (2017) 215-256.
- 33 [12] A.T. Lorenzo, M.L. Arnal, J.J. Sánchez, A.J. Müller, Effect of Annealing Time on  
34 the Self-Nucleation Behavior of Semicrystalline Polymers, *J. Polym. Sci., Part B:  
35 Polym. Phys.* 44 (2006) 1738-1750.
- 36 [13] L. Wang, X. Dong, M. Huang, A.J. Müller, D. Wang, Self-associated Polyamide  
37 Alloys with Tailored Polymorphism Transition and Lamellar Thickening for  
38 Advanced Mechanical Application, *Acs Appl. Mater. Interfaces* 9 (2017)

- 1 19238-19247.
- 2 [14] X. Li, F. Su, Y. Ji, N. Tian, J. Lu, Z. Wang, Z. Qi, L. Li, Influence of the Memory  
3 Effect of a Mesomorphic Isotactic Polypropylene Melt on Crystallization Behavior,  
4 *Soft Matter* 9 (2013) 8579-8588.
- 5 [15] P. Supaphol, J.S. Lin, Crystalline Memory Effect in Isothermal Crystallization of  
6 Syndiotactic Polypropylenes: Effect of Fusion Temperature on Crystallization and  
7 Melting Behavior, *Polymer* 42 (2001) 9617-9626.
- 8 [16] J. Kawabata, G. Matsuba, K. Nishida, R. Inoue, T. Kanaya, Melt Memory Effects  
9 on Recrystallization of Polyamide 6 Revealed by Depolarized Light Scattering and  
10 Small-Angle X-ray Scattering, *J. Appl. Polym. Sci.* 122 (2011) 1913-1920.
- 11 [17] Y. Xu, Y. Wang, T. Xu, J. Zhang, C. Liu, C. Shen, Crystallization Kinetics and  
12 Morphology of Partially Melted Poly(lactic acid), *Polym. Test.* 37 (2014) 179-185.
- 13 [18] W. Zhang, Evaluation of the Effect of Melt Memory on Shear-Induced  
14 Crystallization of Low-Density Polyethylene, *Macromol. Rapid Commun.* 27 (2010)  
15 1067-1072.
- 16 [19] F.A. And, G.C. Alfonso, Lifetime of Shear-Induced Crystal Nucleation  
17 Precursors, *Macromolecules* 38 (2005) 1723-1728.
- 18 [20] L. Sangroniz, D. Cavallo, A. Santamaria, A.J. Müller, R.G. Alamo,  
19 Thermorheologically Complex Self-Seeded Melts of Propylene-Ethylene Copolymers,  
20 *Macromolecules* 50 (2017) 642-651.
- 21 [21] H. Li, X. Sun, J. Wang, S. Yan, J.M. Schultz, On the Development of Special  
22 Positive Isotactic Polypropylene Spherulites, *J. Polym. Sci., Part B: Polym. Phys.* 44  
23 (2006) 1114-1121.
- 24 [22] L. Sangroniz, F. Barbieri, D. Cavallo, A. Santamaria, R.G. Alamo, A.J. Müller,  
25 Rheology of Self-Nucleated Poly( $\epsilon$ -caprolactone) Melts, *Eur. Polym. J.* 99 (2018)  
26 495-503.
- 27 [23] L. Sangroniz, R.G. Alamo, D. Cavallo, A. Santamaría, A. Alegría, Differences  
28 between Isotropic and Self-Nucleated PCL Melts Detected by Dielectric Experiments,  
29 *Macromolecules* 51 (2018) 3663-3671.
- 30 [24] X. Chen, G.D. Wignall, L. He, C. Lopezbarron, R.G. Alamo, SANS Evidence of  
31 Liquid-Liquid Phase Separation Leading to Inversion of Crystallization Rate of  
32 Broadly Distributed Random Ethylene Copolymers, *Macromolecules* 50 (2017)  
33 4406-4414.
- 34 [25] M. Muthukumar, Communication: Theory of Melt-Memory in Polymer  
35 Crystallization, *J. Chem. Phys.* 145 (2016) 821-614.
- 36 [26] X. Li, Z. Ma, F. Su, N. Tian, Y. Ji, J. Lu, Z. Wang, L. Li, New Understanding on  
37 the Memory Effect of Crystallized iPP, *Chin. J. Polym. Sci.* 32 (2014) 1224-1233.
- 38 [27] H. Gao, M. Vadlamudi, R.G. Alamo, W. Hu, Monte Carlo Simulations of Strong  
39 Memory Effect of Crystallization in Random Copolymers, *Macromolecules* 46 (2013)  
40 6498-6506.
- 41 [28] C. Luo, J.U. Sommer, Frozen Topology: Entanglements Control Nucleation and  
42 Crystallization in Polymers, *Phys. Rev. Lett.* 112 (2014) 195702.



- 1 [29] D. Cavallo, F. Azzurri, L. Balzano, S.S. Funari, G.C. Alfonso, Flow Memory and  
2 Stability of Shear-Induced Nucleation Precursors in Isotactic Polypropylene,  
3 *Macromolecules* 43 (2010) 9394-9400.
- 4 [30] K. Cho, D.N. Saheb, J. Choi, H. Yang, Real Time in Situ X-ray Diffraction  
5 Studies on the Melting Memory Effect in the Crystallization of  $\beta$ -Isotactic  
6 Polypropylene, *Polymer* 43 (2002) 1407-1416.
- 7 [31] R. Androsch, B. Wunderlich, Analysis of the Degree of Reversibility of  
8 Crystallization and Melting in Poly(ethylene-co-1-octene), *Macromolecules* 33 (2000)  
9 9076-9089.
- 10 [32] A.M. Gohn, A.M. Rhoades, O. David, A. René, Effect of Melt-Memory on the  
11 Crystal Polymorphism in Molded Isotactic Polypropylene, *Macromol. Mater. Eng.*  
12 303 (2018) 1800148.
- 13 [33] S.N.Vouyiouka, E.K.Karakatsani, C.D.Papaspyrides, *Solid State Polymerization*,  
14 *Prog. Polym. Sci.* 30 (2005) 10-37.
- 15 [34] Z. Yao, W.H. Ray, Modeling and analysis of new processes for polyester and  
16 nylon production, *Aiche Journal* 47 (2001) 401-412.
- 17 [35] L. Chocinski-Arnault, V. Gaudefroy, J.L. Gacougnolle, A. Rivière, Memory  
18 Effect and Crystalline Structure in Polyamide 11, *J. Polym. Sci., Part B: Polym. Phys.*  
19 41 (2002) 777-785.
- 20 [36] N. Vasanthan, "Orientation Induced Memory Effect" in Polyamides and the  
21 Relationship to Hydrogen Bonding, *J. Appl. Polym. Sci.* 90 (2003) 772-775.
- 22 [37] Y.P. Khanna, R. Kumar, A.C. Reimschuessel, Memory effects in polymers. III.  
23 Processing history vs. crystallization rate of nylon 6—comments on the origin of  
24 memory effect, *Polym. Eng. Sci* 28 (1988) 1607-1611.
- 25 [38] Y.P. Khanna, A.C. Reimschuessel, Memory effects in polymers. I. Orientational  
26 memory in the molten state; its relationship to polymer structure and influence on  
27 recrystallization rate and morphology, *J. Appl. Polym. Sci.* 35 (1988) 2259-2268.
- 28 [39] Y.P. Khanna, A.C. Reimschuessel, A. Banerjee, C. Altman, Memory effects in  
29 polymers. II. Processing history vs. crystallization rate of nylon 6—observation of  
30 phenomenon and product behavior, *Polym. Eng. Sci* 28 (1988) 1600-1606.
- 31 [40] L. Wang, X. Dong, M. Huang, D. Wang, Transient Microstructure in Long  
32 Alkane Segment Polyamide: Deformation Mechanism and Its Temperature  
33 Dependence, *Polymer* 97 (2016) 217-225.
- 34 [41] L. Wang, X. Dong, X.R. Wang, G.Y. Zhu, H.Q. Li, D.J. Wang, High Performance  
35 Long Chain Polyamide/Calcium Silicate Whisker Nanocomposites and the Effective  
36 Reinforcement Mechanism, *Chin. J. Polym. Sci.* 34 (2016) 991-1000.
- 37 [42] P. Zhu, X. Dong, Y. Cao, L. Wang, X. Liu, Z. Wang, D. Wang, The Brill  
38 Transition in Polyether- b -amide Segmented Copolymers and Composition  
39 Dependence, *Eur. Polym. J.* 93 (2017) 334-346.
- 40 [43] P. Zhu, X. Dong, D. Wang, Strain-Induced Crystallization of Segmented  
41 Copolymers: Deviation from the Classic Deformation Mechanism, *Macromolecules*  
42 50 (2017) 3911-3921.

- 1 [44] Y. Gao, X. Dong, L. Wang, G. Liu, X. Liu, C. Tuinea-Bobe, B. Whiteside, P.  
2 Coates, D. Wang, C.C. Han, Flow-Induced Crystallization of Long Chain Aliphatic  
3 Polyamides under a Complex Flow field: Inverted Anisotropic Structure and  
4 Formation Mechanism, *Polymer* 73 (2015) 91-101.
- 5 [45] S. Dong, P. Zhu, J. Liu, D. Wang, X. Dong, Thermal Treatment Effects on the  
6 Microstructure and Tensile Properties of Transparent Polyamides, *Acta Polym. Sin.* 50  
7 (2019) 189-197.
- 8 [46] C. Suchocki, R. Molak, Rheological Properties of Polyamide: Experimental  
9 Studies and Constitutive Modeling, *Chin. J. Polym. Sci.* 37 (2019) 178-188.
- 10 [47] D. Wang, C. Shao, B. Zhao, L. Bai, X. Wang, T. Yan, J. Li, G. Pan, L. Li,  
11 Deformation-Induced Phase Transitions of Polyamide 12 at Different Temperatures:  
12 An in Situ Wide-Angle X-ray Scattering Study, *Macromolecules* 43 (2010)  
13 2406-2412.
- 14 [48] M.V. Drongelen, A. Stroeks, G.W.M. Peters, Kinetics of the Deformation  
15 Induced Memory Effect in Polyamide-6, *Eur. Polym. J.* 72 (2015) 296-308.
- 16 [49] Y. Wu, Y. Xu, D. Wang, Z. Ying, S. Weng, D. Xu, J. Wu, FT-IR spectroscopic  
17 investigation on the interaction between nylon 66 and lithium salts, *J. Appl. Polym.*  
18 *Sci.* 91 (2004) 2869-2875.
- 19 [50] D.J. Skrovanek, S.E. Howe, P.C. Painter, M.M. Coleman, Hydrogen Bonding in  
20 Polymers: Infrared Temperature Studies of An Amorphous Polyamide,  
21 *Macromolecules* 18 (1985) 1676-1683.
- 22 [51] D.J. Skrovanek, P.C. Painter, M.M. Coleman, Hydrogen Bonding in Polymers. 2.  
23 Infrared Studies of Nylon 11, *Macromolecules* 19 (1986) 699-705.
- 24 [52] M. Tsuboi, Some Problems in the Infrared Spectra of Polypeptides and  
25 Polynucleotides, *Biopolym. Symp.* 13 (1964) 527-47.
- 26 [53] A. Davis, D.W. Kuehn, M. Starsinic, M.M. Coleman, P.C. Painter, R.W. Snyder,  
27 Concerning the Application of FT-IR to the Study of Coal: A Critical Assessment of  
28 Band Assignments and the Application of Spectral Analysis Programs, *Applied*  
29 *Spectroscopy* 35 (1981) 475-485.
- 30 [54] W.F. Maddams, The Scope and Limitations of Curve Fitting, *Applied*  
31 *Spectroscopy* 34 (1980) 245-267.
- 32 [55] M.M. Coleman, D.J. Skrovanek, P.C. Painter, Hydrogen Bonding in Polymers:  
33 III Further Infrared Temperature Studies of Polyamides, *Macromol Symp* 5 (2011)  
34 21-33.
- 35 [56] W.H. Moore, S. Krimm, Vibrational analysis of peptides, polypeptides, and  
36 proteins. II. beta-poly(L-alanine) and beta-poly(L-analyglycine), *Biopolymers* 15  
37 (1976) 2439-2464.
- 38 [57] M.M. Coleman, M. Sobkowiak, G.J. Pehlert, P.C. Painter, T. Iqbal, Infrared  
39 Temperature Studies of a Simple Polyurea, *Macromolecular Chemistry & Physics* 198  
40 (1997) 117-136.
- 41 [58] D. Garcia and H. W. Starkweather, Jr., Hydrogen Bonding in Nylon 66 and  
42 Model Compounds. *J. Polym. Sci., Polym. Phys. Ed.*, 23, 557-575 (1985).

- 1 [59] N.A. Jones, E.D.T. Atkins, M.J. Hill, S.J. Cooper, L. Franco, Polyamides with a  
2 Choice of Structure and Crystal Surface Chemistry. Studies of Chain-Folded Lamellae  
3 of Nylons 8 10 and 10 12 and Comparison with the Other 2N 2(N + 1) Nylons 4 6 and  
4 6 8, *Macromolecules* 30 (1997) 3569-3578.
- 5 [60] N.A. Jones, E.D.T. Atkins, M.J. Hill, S.J. Cooper, L. Franco, Chain-folded  
6 lamellar crystals of aliphatic polyamides. Investigation of nylons 4 8, 4 10, 4 12, 6 10,  
7 6 12, 6 18 and 8 12, *Polymer* 38 (1997) 2689-2699.
- 8 [61] M. Trujillo, M.L. Arnal, A.J. Müller, E. Laredo, S. Bredeau, D. Bonduel, P.  
9 Dubois, Thermal and Morphological Characterization of Nanocomposites Prepared by  
10 in-Situ Polymerization of High-Density Polyethylene on Carbon Nanotubes,  
11 *Macromolecules* 40 (2007) 6268-6276.
- 12 [62] M. Trujillo, M.L. Arnal, A.J. Müller, S. Bredeau, D. Bonduel, P. Dubois, I.W.  
13 Hamley, V. Castelletto, Thermal Fractionation and Isothermal Crystallization of  
14 Polyethylene Nanocomposites Prepared by in Situ Polymerization, *Macromolecules*  
15 41 (2008) 2087-2095.

## Highlights

- The relationship between memory effect and hydrogen bonding was investigated.
- Hydrogen bonding strength between N-H groups decreases with  $T_s$  values.
- The width of *Domain IIa* increases with the density of amide groups in polyamides.

Journal Pre-proof

The manuscript was written through contributions of all authors. All authors have given approval to the final version of the manuscript. X. Liu and Y. Wang contributed equally to this work.

Journal Pre-proof

**Declaration of interests**

The authors declare that they have no known competing financial interests or personal relationships that could have appeared to influence the work reported in this paper.

The authors declare the following financial interests/personal relationships which may be considered as potential competing interests: